Check for updates

Controllable permittivity in 3D Fe$_3$O$_4$/CNTs network for remarkable microwave absorption performances

Lingyu Zhu,† Xiaojun Zeng, [ID] †* Meng Chen and Ronghai Yu*

Carbon-based magnetic composites are promising alternatives to pure magnetic nanoparticles (MO$_x$, M = Fe, Co, Ni) and spinel ferrites (MFe$_2$O$_4$, M = Fe, Co, Ni, Mn, Zn) as electromagnetic (EM) wave absorption materials, which however suffer from complex processes and have poor microwave absorption properties. Herein, we anchored Fe$_3$O$_4$ porous spheres onto carbon nanotubes (CNTs) *via* a simple solvothermal method. The formed Fe$_3$O$_4$/CNTs nanocomposites show a three-dimension (3D) network. The improved effective bandwidth (3.9 GHz) and, more importantly, remarkable EM microwave absorption performances (−51 dB at 5.52 GHz) are observed in 3D Fe$_3$O$_4$/5 wt% CNTs nanocomposites. The enhanced microwave absorption performances are attributed to the high surface areas and porous structure of magnetic Fe$_3$O$_4$ spheres, which presented a good synergetic role with CNTs. Furthermore, the controllable permittivity in nanocomposites was developed by adjusting the CNT content, which balanced the permeability to obtain a good impedance matching. This work demonstrates a simple approach to enhancing the microwave absorption performances of EM wave absorption materials.

1. Introduction

Many efforts have been devoted to develop high-efficiency electromagnetic (EM) microwave absorption materials because of their great potential applications in military (improvement of radar invisible of aircrafts, tanks and targets) and civil (diminution of unprecedented EM radiation and betterment of EM compatibility) fields.[1–5] One type of microwave absorption materials, magnetic loss materials, *e.g.* magnetic nanoparticles (MO$_x$, M = Fe, Co, Ni)[6–8] and spinel ferrites (MFe$_2$O$_4$, M = Fe, Co, Ni, Mn, Zn),[9–12] are mostly used as efficient wave absorption materials. Among these magnetic loss materials, Fe$_3$O$_4$ has received much attention as a result of their proper microwave absorption abilities, good environmental benignity and low cost. For example, the minimum reflection loss (RL) value of triangular Fe$_3$O$_4$ nanoplates has been reported to be −32.1 dB at 11.7 GHz.[13] The epoxy/Fe$_3$O$_4$-PPy nanocomposites exhibit a minimum RL of −35.7 dB with a sample thickness of 1.7 mm.[14] However, the high density and poor wave absorption properties block their large-scale applications. The other type of microwave absorption materials, dielectric loss materials, *e.g.* MnO$_2$,[15] CuS,[16] SiC,[17] BaTiO$_3$,[18] single negative materials[19] and carbon-based materials,[20,21] are also promising in EM microwave absorption fields. Nevertheless, it is hard to reach a good impedance matching in these unilateral magnetic loss or dielectric loss materials by adjusting the complex effective permittivity (ε_r) and permeability (μ_r).[22,23] The carbon-based magnetic composites have attracted much research attention as EM microwave absorption materials by virtue of their good magnetic and dielectric properties along with lightweight and chemical stability.[24]

Lightweight, wide-absorption bandwidth and high absorption intensity, are indispensable for a real application of carbon-based magnetic composites. Among all the carbon materials, the multiwalled carbon nanotubes (MWCNTs) have attracted considerable attention for their low density, high chemical stability and interesting electrical properties, especially tuning their relatively high permittivity is an important approach for achieving a good impedance matching.[25–27] Recently, several MWCNTs-based magnetic nanocomposites have been reported to exhibit good EM microwave absorption properties. For example, MWCNTs/Fe composite possessed a minimum RL of −39 dB at 2.68 GHz with a sample thickness of 4.27 mm.[28] MWCNTs/Fe$_3$O$_4$ hybrid reached a RL of −35.8 dB at 8.56 GHz and with a bandwidth of 2.32 GHz.[29] Moreover, the γ-Fe$_2$O$_3$–MWNTs/PBO composites, fabricated by loading CNTs with magnetic γ-Fe$_2$O$_3$ particles and premixing γ-Fe$_2$O$_3$–MWNTs and PHA in solution followed by *in situ* cyclodehydration, also obtained optimal minimum RL of −32.7 dB.[30] However, few mitigation strategies have been able to control the complex effective ε_r to improve the microwave absorption properties of carbon-based magnetic composites. More efforts are in urgent need to clarify responsible mechanisms for their poor absorption performances, and create effective solutions.

School of Materials Science and Engineering, Beihang University, Beijing 100191, China. E-mail: Xiaojun-Zeng@buaa.edu.cn; rhyu@buaa.edu.cn

† These authors contributed equally to this work.

Here, we report a precise adjustment of ε_r for carbon-based magnetic composites by anchoring uniform Fe_3O_4 porous spheres onto carbon nanotubes (CNTs), marked as Fe_3O_4/CNTs, through a facile one-pot solvothermal method, which is time and energy-saving. A top-level microwave absorption performance of -51 dB at 5.52 GHz was achieved on Fe_3O_4/5 wt% CNTs nanocomposites with a three-dimension (3D) network structure. The modified ε_r presented improved impedance matching in these nanocomposites, possibly attributed to the good synergetic effects between magnetic Fe_3O_4 porous spheres and lightweight CNTs. Moreover, the high surface areas and porous structure of magnetic Fe_3O_4 spheres also contribute to the enhanced microwave absorption performances with a relatively high bandwidth of 3.9 GHz (RL < -10 dB).

2. Methods

2.1. Preparation of Fe_3O_4/CNTs

Firstly, ferric chloride hexahydrate ($FeCl_3 \cdot 6H_2O$, 1.08 g) was added into 32 mL polyacrylamides (PAM, 12.5 g L^{-1}) aqueous solution. Then, sodium citrate (2 g), urea (0.36 g) and CNTs (5 wt%, pre-treated by nitric acid) were successively added into the above solution under magnetic stirring and ultrasonic treatment for 20 min. Afterwards, the obtained mixture was transferred into a 50 mL Teflon-lined stainless steel and then heated at 180 °C for 8 h in an electric oven. After cooling the cave to room temperature, the products were collected by centrifugation, washed subsequently with deionized water and absolute ethanol for ten times and then dried at 60 °C under vacuum for one day. To understand the effects of CNTs content on microwave absorption performances, four samples containing 0, 3, 5, 7 wt% CNTs (marked as Fe_3O_4, Fe_3O_4/3 wt% CNTs, Fe_3O_4/5 wt% CNTs and Fe_3O_4/7 wt% CNTs), were synthesized through the same process as described above.

2.2. Characterization

The phase structure of samples was performed on X-ray diffraction (XRD) using a Rigaku D/max 2500PC X-ray diffractometer with Cu K$_\alpha$ radiation. The microstructures and morphologies of samples were observed by scanning electron microscopy (SEM, JSM-7500F, JEOL) and transmission electron microscopy (TEM, JEM-2100, JEOL). Nitrogen absorption and desorption isotherms were obtained at 77 K on a Quanta chrome surface and pore size analyzer to characterize the Brunauer–Emmett–Teller (BET) surface area of the samples. An X-ray photoelectron spectroscope (XPS, ESCALAB 250 X_i) with an Al K$_\alpha$ excitation source was applied to probe the surface compositions and valence states of samples. The hysteresis loops of samples were conducted on a vibrating sample magnetometer (VSM, Lakeshore 7307).

2.3. Wave absorption measurements

All microwave absorption measurements were conducted on an Agilent N5230C network analyzer at the frequency range of 2–18 GHz, as described in our previous work.[31] To prepare the measured samples, products (50 wt%) and paraffin wax (50

wt%) were mixed to form a uniform composites. The obtained homogeneous mixture was compressed into toroidal shaped with internal diameter of 3 mm, outside diameter of 7 mm, and thickness of 3 mm. The measured effective permittivity (ε_r) and permeability (μ_r) were converted to reflection loss (RL) according to the transmission line theory as following equation:[32]

$$Z_{in} = Z_0(\mu_r/\varepsilon_r)^{1/2} \tanh[j(2\pi fd/c)(\mu_r\varepsilon_r)^{1/2}] \qquad (1)$$

$$RL = 20 \log(Z_{in} - Z_0)/(Z_{in} + Z_0) \qquad (2)$$

where Z_{in} and Z_0 are the input impedance and free-space impedance, respectively. μ_r and ε_r are the effective relative complex permeability and permittivity, respectively. d is the absorber thickness, f is the frequency of EM wave, and c is the light velocity.

3. Results and discussion

3.1. Characterization of the Fe_3O_4/CNTs composites

To determine the optimum conditions for the microwave absorption performances of Fe_3O_4/CNTs nanocomposites, different ratios of Fe_3O_4 and CNTs were examined. As can be seen in the XRD patterns (Fig. 1a), the diffraction peak at 26.2° in Fe_3O_4/CNTs composites suggests the addition of CNTs. The rest of diffraction peaks in all samples match well with the crystal planes of the face-centered cubic Fe_3O_4 phase (JCPDS, no. 99-0073), revealing that the as-prepared Fe_3O_4 are well-crystallized and high purity. This is also proved by the XPS spectra (Fig. 1b and c), in which signals of Fe and C element in Fe_3O_4/5 wt% CNTs composites are observed. The Fe 2p spectrum (Fig. 1b) contains only two characteristic peaks of Fe 2p$_{1/2}$ (723.5) and 2p$_{3/2}$ (709.9 eV), and without satellite peak, indicating the formation of pure Fe_3O_4 phase.[33] The C 1s spectrum (Fig. 1c) consists of four deconvoluted peaks that correspond to C–C/C=C (284.6 eV), C–O/C–O–C (285.6 eV), C=O (287.7 eV) and O–C=O (290.1 eV), respectively.[34,35] These heteroatoms are formed during the pretreatment of CNTs. The N_2 adsorption–desorption isotherm of Fe_3O_4/5 wt% CNTs (Fig. 1d) shows a typical type-IV isotherm with obvious hysteresis loop at a relative pressure range of 0.45–0.95, which implying the mesoporous structure of the Fe_3O_4 spheres in composites. Furthermore, the BET surface area of the composites is 92 cm^2 g^{-1} and the pore size is about 4.3 nm. It has been confirmed that the high surface areas and porous structure are effective for EM microwave absorption.[36,37]

Fig. 2 shows the representative SEM (Fig. 2a–d) and TEM (Fig. 2e–h) images of the Fe_3O_4 sample and Fe_3O_4/CNTs composites. It is clear that all of the Fe_3O_4 particles in Fe_3O_4 sample are spherical and monodispersed with an obvious porous structure (Fig. 2a and e). Furthermore, the Fe_3O_4 porous spheres have a uniform distribution of particle size, which can be ascribed to the modulating effect of surfactant PAM. As presented in Fig. 2b–d and f–h, Fe_3O_4 porous spheres are anchored onto CNTs, and the high-conductivity CNTs across the whole composites and tightly bind the Fe_3O_4 spheres, resulting in a three-dimension (3D) network, which can bring
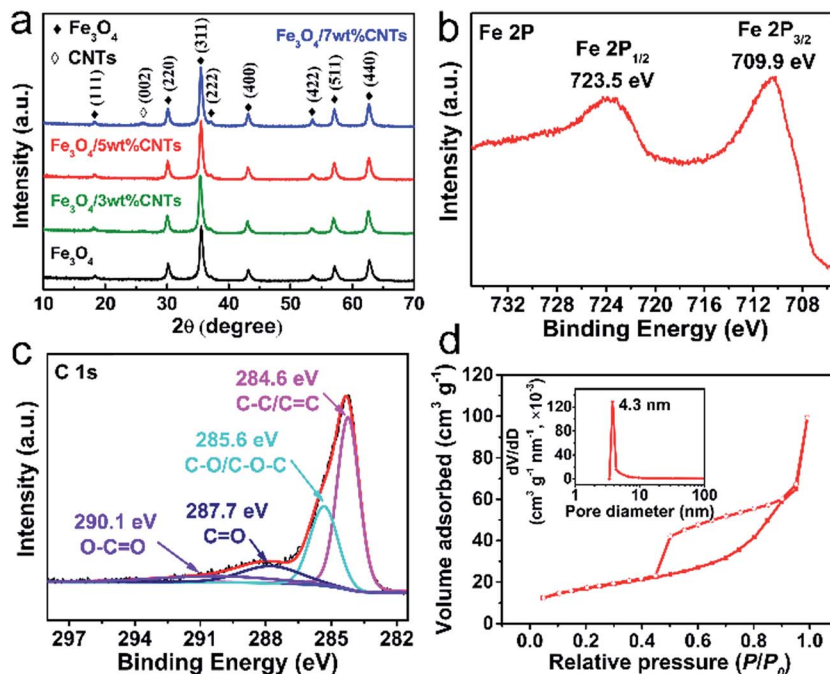
Fig. 1 The XRD patterns of samples (a). The XPS spectra of Fe 2p (b) and C 1s (c), and N_2 absorption–desorption isotherms (d) of Fe_3O_4/5 wt% CNTs composites.

an enhanced permittivity, as reported in the previous works.[38,39] It is noteworthy that the Fe_3O_4 spheres in Fe_3O_4/CNTs composites have rougher surface, smaller size and more interfaces than porous spheres in Fe_3O_4 sample, which also improve the bonding strength and interaction between Fe_3O_4 and CNTs. The abundant oxygen-containing groups (–COOH, –OH) existing on the surface of CNTs are beneficial for binding the Fe^{3+} *via* the electrostatic interaction. As the reaction proceeds, the initially formed Fe_3O_4 crystals are anchored on the surface of CNTs and grow to be porous spheres, as shown in the inset of Fig. 2g. The incident EM microwaves could be dissipated and absorbed as a result of being repeatedly scattered and reflected between the interfaces. Thus, the plentiful interfaces exhibiting

in composites can make contributions to microwave absorption properties through the interface loss.[37,40] However, the excessive CNTs in Fe_3O_4/7 wt% CNTs composites show agglomeration phenomenon which may do harm to their microwave absorption performances, as will be confirmed below.

3.2. Magnetic properties of the Fe_3O_4/CNTs composites

It is generally accepted that the magnetization property highly affects the microwave absorption ability of an absorber due to the obvious magnetic loss behavior. As shown in the hysteresis loops (Fig. 3), all samples exhibit typical magnetization hysteresis behaviors of superparamagnetic materials, identifying the good intrinsic magnetic properties with high saturation
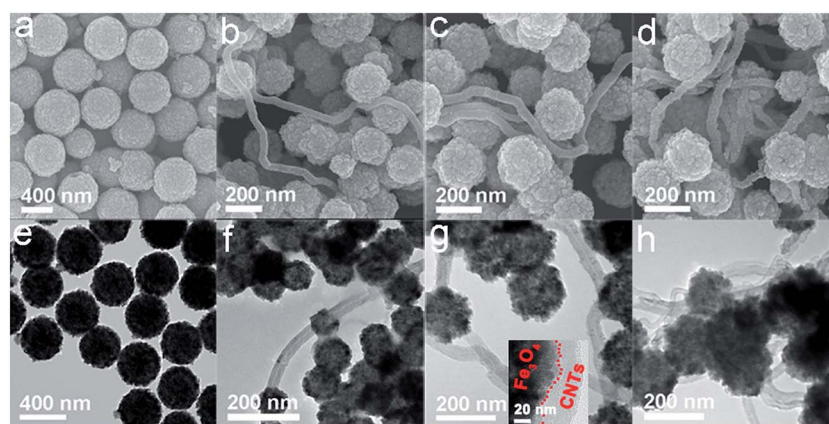

Fig. 2 The SEM and TEM images of Fe_3O_4 sample (a and e), Fe_3O_4/3 wt% CNTs (b and f), Fe_3O_4/5 wt% CNTs (c and g) and Fe_3O_4/7 wt% CNTs (d and h) composites.
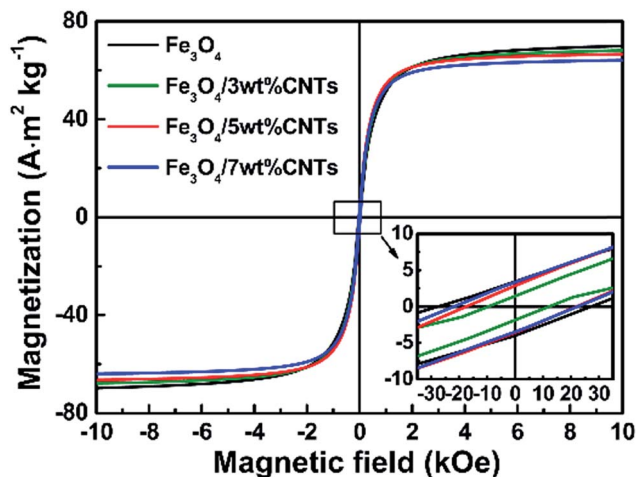
Fig. 3 The room-temperature hysteresis loops of the Fe_3O_4 sample and Fe_3O_4/CNTs composites.

magnetization (M_s) and low coercivity (H_c), which bring a good permeability and magnetic loss and further make contribution to the microwave absorption, as discussed in our previous work.[31] The M_s values are decreased with the increase of CNTs content in composites, which resulting from the decrease of magnetic Fe_3O_4 phases. In addition, Fe_3O_4 sample and Fe_3O_4/CNTs composites show very low H_c values, which can be ascribed to the high particle symmetry of uniform Fe_3O_4 porous spheres.

3.3. Microwave absorption performances of the Fe_3O_4/CNTs composites

The EM absorption performance of an absorber is evaluated by their EM parameters including complex effective permittivity

($\varepsilon_r = \varepsilon' - j\varepsilon''$) and permeability ($\mu_r = \mu' - j\mu''$), where the real parts (ε' and μ') represent the storage capability and the imaginary parts (ε'' and μ'') signify the dissipation ability of EM microwave energies.[41] Fig. 4 shows the measured μ_r and ε_r, calculated magnetic loss (tan δ_μ) and dielectric loss (tan δ_ε) for the Fe_3O_4 sample and Fe_3O_4/CNTs composites. The similar μ' and μ'' values (Fig. 4a and b) for all samples over the whole frequency range illustrating their alike ability to store and dissipate magnetic energies, which owing to the high mass percentage of magnetic Fe_3O_4 in the composites. It is worth noting that the ε' and ε'' values (Fig. 4d and e) of samples improve greatly with the increasing of CNTs content, demonstrating that the dielectric loss and storage capability have been obviously enhanced due to the increased electric polarization and conductivity resulting from the proper CNTs addition.[42] Meanwhile, the ε_r can be controlled by regulating the CNTs content. It should, however, be taken into account that the Fe_3O_4/7 wt% CNTs show a slightly lower ε' and ε'' values than Fe_3O_4/5 wt% CNTs, which may be attributed to the agglomeration of excess CNTs.

To help analyze the principle reasons of microwave absorption of the samples, the tan δ_μ(μ''/μ') and tan δ_ε($\varepsilon''/\varepsilon'$) are calculated based on the measured ε_r and μ_r. The slight difference in values and tendency of magnetic loss tan δ_μ (Fig. 4c) among four samples agrees well with the above analysis of μ' and μ''. Notably, the Fe_3O_4/CNTs composites maintain a stronger and more efficient dielectric loss tan δ_ε (Fig. 4f) than Fe_3O_4 samples. Especially, the Fe_3O_4/5 wt% CNTs composites show the strongest dielectric loss, which may bring an excellent microwave absorption performance, as will be discussed below.

The high dielectric loss of Fe_3O_4/CNTs composites encouraged us to deeply explore their mechanisms through the theory of Debye dipolar relaxation. According to the Debye theory, ε' and ε'' follow the equation:[43]
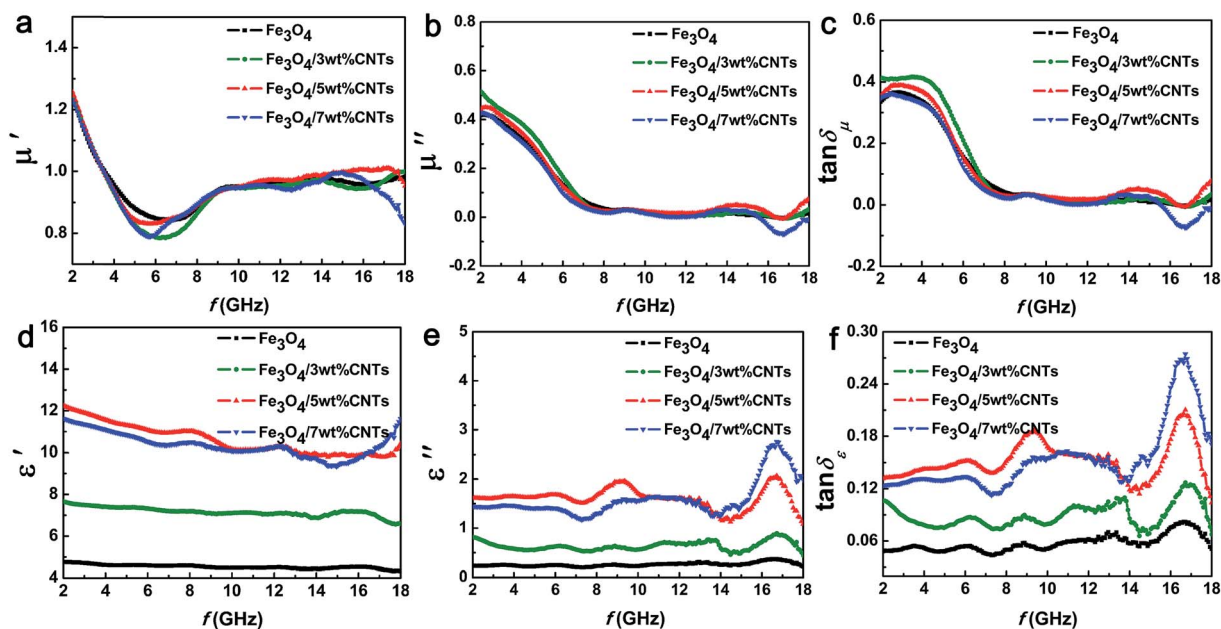

Fig. 4 The measured μ_r (a and b) and ε_r (d and e) of Fe_3O_4 sample and Fe_3O_4/CNTs composites. The corresponding tan δ_μ (c) and tan δ_ε (f) of those samples. The microwave absorption measurements are performed at the frequency range of 2–18 GHz.
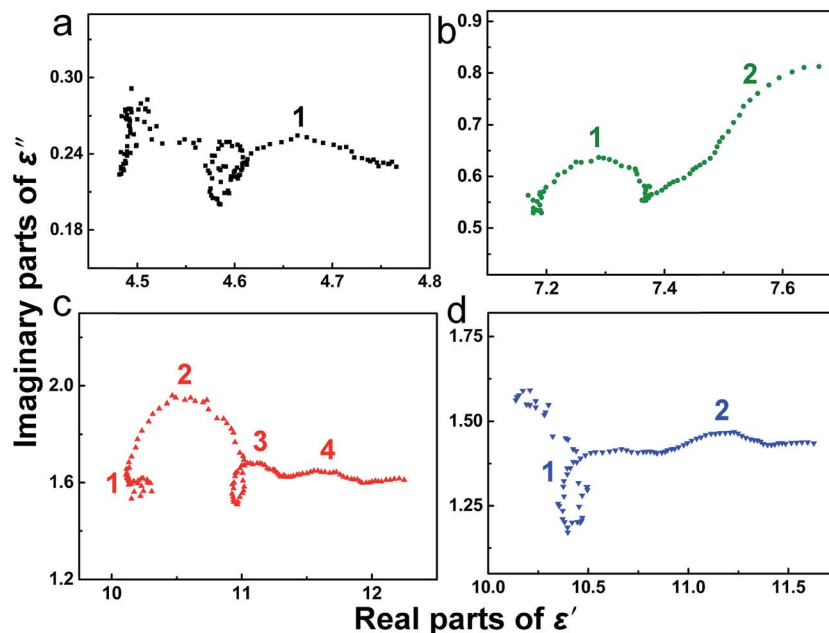
Fig. 5 Plots of ε'–ε'' for Fe_3O_4 sample (a), Fe_3O_4/3 wt% CNTs (b), Fe_3O_4/5 wt% CNTs (c) and Fe_3O_4/7 wt% CNTs (d) composites.

$$(\varepsilon' - \varepsilon_\infty)^2 + (\varepsilon'')^2 = (\varepsilon_s - \varepsilon_\infty)^2 \qquad (3)$$

where ε_∞ and ε_s are the relative permittivity and static permittivity at high-frequency limit, respectively. Hence, the ε'–ε'' curves deduced from eqn (3) would be a semicircle, which is donated as Cole–Cole semicircle and corresponds to one Debye relaxation caused by heterogeneous interface polarization.[44,45] The ε'–ε'' curves are displayed in Fig. 5. It shows that only one distinguishable Cole–Cole semicircle can be observed in Fe_3O_4 sample (Fig. 5a), implying that there is sole relaxation process for Fe_3O_4 sample. It is exciting to find that Fe_3O_4/CNTs composites achieved more semicircles, confirming that the addition of CNTs endows these composites with multiple

dielectric relaxation processes which are ascribed to the interface polarization generated at the interfaces between CNTs and Fe_3O_4 porous spheres. Surprisingly, the Fe_3O_4/5 wt% CNTs composites show four conspicuous Cole–Cole semicircles (Fig. 5c), indicating four dielectric relaxation processes, which makes significant contribution to the enhancement of EM microwave absorption performance. The enhanced polarization relaxation is mostly coming from the defects in CNTs, which can act as polarization centers. Furthermore, the abundant oxygenic functional groups, as found in above XPS spectra, can produce electronic dipole polarization caused by the different electronegativity of heteroatoms.[46] Of note, the semicircles in all ε'–ε'' curves are disordered, revealing that besides the dielectric
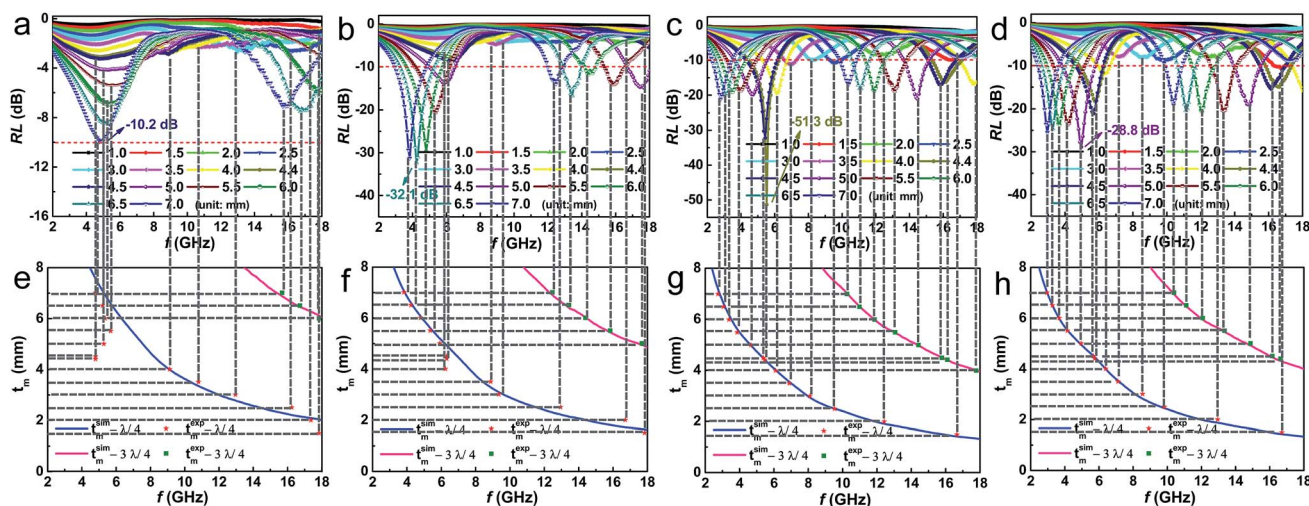

Fig. 6 RL curves of Fe_3O_4 sample (a), Fe_3O_4/3 wt% CNTs (b), Fe_3O_4/5 wt% CNTs (c) and Fe_3O_4/7 wt% CNTs (d) composites. The dependence of t_m on f_m for Fe_3O_4 sample (e) and Fe_3O_4/CNTs composites (f–h) at wavelengths of $\lambda/4$ and $3\lambda/4$.

Table 1 Microwave absorption performances of various carbon-based magnetic composites in previous reports compared with Fe_3O_4/5 wt% CNTs composites[a]

	RL_{min} (dB)	Frequency range (GHz)	Effective bandwidth (GHz) (RL < −10 dB)	Thickness (mm)	Weight fraction (wt%)	Ref.
CNTs/Co	−60.4	12.8–18.0	5.2	1.81	20	46
NiO@GO	−59.6	12.48–16.72	4.24	1.7	25	47
Fe_3O_4/5 wt% CNTs	−51.3	4.4–6.3, 15.3–17.3	3.9	4.4	50	This work
NiFe@C nanocubes@GO	−51.0	8.5–12.6	4.1	2.8	30	48
Carbon@Fe@Fe_3O_4	−40.0	8.6–13.8	5.2	1.5	50	49
NWCNTs/Fe	−39.0	2.5–7.5	5.0	4.3	60	28
Fe-filled CNT/epoxy	−31.7	14.7–11.8	2.9	1.0	10	50
Fe_3O_4@Carbon	−29.0	13.0–18.0	5.0	5.0	50	43
Fe_3O_4/polypyrrole/CNTs	−25.9	8.0–12.5	4.5	3.0	20	51
CNT@Fe@SiO_2	−22.3	7.5–11.0	3.5	3.0	50	52
PANI/Fe_3O_4/MWCNT	−16.0	8.0–15.0	7.0	4.0	20	53

[a] Note: the exact RL_{min} and effective bandwidths were not presented in some references, thus, those values were dug out according to the RL–f curves.
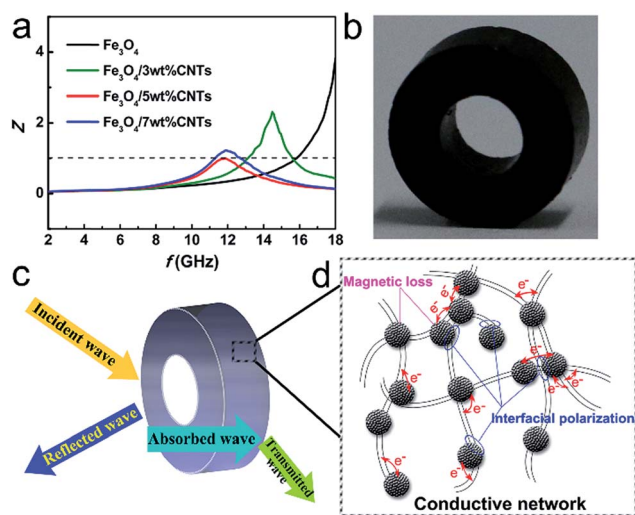

Fig. 7 (a) The frequency-dependent Z values of Fe_3O_4 sample and Fe_3O_4/CNTs composites. (b) Image of real product for absorber. (c and d) Scheme of primary EM microwave attenuation processes involved in Fe_3O_4/CNTs composites absorber.

relaxation, other mechanisms such as conducting loss may also contribute to the permittivity plot.

Reflection loss (RL), effective bandwidth (RL < −10 dB), and thickness of sample are important criterions for evaluating the application prospects of microwave absorption materials. Fig. 6 shows a comparison of RL values (calculated from eqn (1) and (2)) in frequency range of 2–18 GHz for Fe_3O_4 sample and Fe_3O_4/CNTs composites with coating thickness of 1–7 mm. It can be seen from Fig. 6a that the Fe_3O_4 product shows weak wave absorption ability with the minimum RL value of −10.2 dB and a large sample thickness of 7 mm. In contrast, the Fe_3O_4/CNTs composites exhibit good wave absorption ability (Fig. 6b–d). Markedly, Fe_3O_4/5 wt% CNTs composites present an unexpected high microwave absorption performance with a minimum RL value of −51.32 dB at 5.52 GHz and a thinner sample thickness of 4.4 mm, which outperforms the

benchmark Fe_3O_4 sample and also surpass most contemporaries reported, as summarized in Table 1. In addition, the effective bandwidth of Fe_3O_4/5 wt% CNTs composites reach a relatively high value of 3.9 GHz. The top-level microwave absorption performances of Fe_3O_4/5 wt% CNTs composites further underline the good polarization relaxation and strong dielectric loss of the material.

Noticeably, with the increasing of sample thickness, the absorption peaks for Fe_3O_4/CNTs composites become sharper and matching frequency (f_m) shift to lower frequency. These results are consistent with the quarter-wavelength cancelation law, $t_m = n\lambda/4 = nc/(4f_m(|\mu_r||\varepsilon_r|)^{1/2})$ ($n = 1, 3, 5,...$), where t_m is matching thickness, λ is the wavelength of EM wave and c is the velocity of light in a vacuum.[45] It is well established that the RL will reach the maximum value if t_m and f_m satisfy this equation.[51,53] The experimental matching thickness (t_m^{exp}) vs. the peak frequency are extracted from RL curves (Fig. 6a–d) and marked as red asterisks and green squares, respectively. From the above equation, the simulation of t_m (t_m^{sim}) vs. f_m for Fe_3O_4 sample and Fe_3O_4/CNTs composites are depicted in Fig. 6e–h. As expected, the scatter symbols in t_m^{sim} vs. f_m curves of Fe_3O_4/5 wt% CNTs composites (Fig. 6g) are exactly situated around the $\lambda/4$ and $3\lambda/4$ curves, meaning that the correlation between t_m and f_m for EM wave absorption of samples agrees well with the quarter-wavelength matching conditions.

To further clarify the responsible mechanisms and Fe_3O_4/CNTs composites' contribution for EM microwave absorption, the impedance matching of samples are analyzed. Good impedance matching means the value of Z ($|Z_{in}/Z_0|$) equal or close to 1 for achieving zero reflection at the air-absorber interface.[22,31] The Z value of Fe_3O_4/5 wt% CNTs composite (Fig. 7a) is almost equal to 1, suggesting the good impedance matching in those materials, which results in their excellent microwave absorption performances. The Fe_3O_4/CNTs composites absorber (Fig. 7b) can attenuate almost all the EM microwave (Fig. 7c) due to the strong dielectric loss including interfacial polarization and hopping of electrons (Fig. 7d), and the magnetic loss from natural resonance and exchange

resonance of Fe_3O_4 porous spheres. Finally, the synergistic effects of the good intrinsic magnetic properties arising from the Fe_3O_4 porous spheres and the good polarization relaxation and strong dielectric loss arising from the CNTs also greatly contribute to the excellent microwave absorption performances.

4. Conclusions

In summary, we demonstrated a facile method for one-pot synthesis of Fe_3O_4/CNTs composites with excellent microwave absorption performances. The uniform magnetic Fe_3O_4 porous spheres were anchored onto CNTs to form a 3D network. The permittivity in composites could be well tuned by adjusting the CNTs content. The good impedance matching, arising from the synergistic effects between the magnetic Fe_3O_4 spheres and high-conductivity CNTs, resulting in the top-level microwave absorption performances with a minimum RL value of -51 dB at 5.52 GHz and a thinner sample thickness of 4.4 mm as well as an effective bandwidth of 3.9 GHz (RL < -10 dB) for Fe_3O_4/CNTs composites. This work presented a simple approach to enhancing the microwave absorption performances of Fe_3O_4/CNTs composites and promoted their potential application in the field of high-performance EM wave materials.

Acknowledgements

References

1 J. W. Liu, R. C. Che, H. J. Chen, F. Zhang, F. Xia, Q. S. Wu and M. Wang, *Small*, 2012, **8**, 1214–1221.

2 T. Xia, C. Zhang, N. A. Oyler and X. B. Chen, *Adv. Mater.*, 2013, **25**, 6905–6910.

3 G. B. Sun, B. X. Dong, M. H. Cao, B. Q. Wei and C. W. Hu, *Chem. Mater.*, 2011, **23**, 1587–1593.

4 C. Alippi, *CAAI Transactions on Intelligence Technology*, 2016, **1**, 1–3.

5 H. Y. Jin, Q. Chen, Z. X. Chen, Y. Hu and J. W. Zhang, *CAAI Transactions on Intelligence Technology*, 2016, **1**, 104–113.

6 H. C. Yu, L. C. Hsu, T. H. Chang and Y. Y. Li, *Dalton Trans.*, 2012, **41**, 723–726.

7 C. Z. He, S. Qiu, X. Z. Wang, J. R. Liu, L. Q. Luan, W. Liu, M. Itosh and K. I. Machida, *J. Mater. Chem.*, 2012, **22**, 22160–22166.

8 G. X. Tong, Q. Hu, W. H. Wu, W. Li, H. S. Qian and Y. Liang, *J. Mater. Chem.*, 2012, **22**, 17494–17504.

9 S. L. Zhang, Q. Z. Jiao, Y. Zhao, H. S. Li and Q. Wu, *J. Mater. Chem. A*, 2014, **2**, 18033–18039.

10 W. M. Zhu, L. Wang, R. Zhao, J. W. Ren, G. Z. Lu and Y. Q. Wang, *Nanoscale*, 2011, **3**, 2862–2864.

11 H. M. Xiao, X. M. Liu and S. Y. Fu, *Compos. Sci. Technol.*, 2006, **66**, 2003–2008.

12 C. H. Peng, H. W. Wang, S. W. Kan, M. Z. Shen, Y. M. Wei and S. Y. Chen, *J. Magn. Magn. Mater.*, 2004, **284**, 113–119.

13 X. Liu, K. Y. Cao, Y. Z. Chen, Y. T. Ma, Q. F. Zhang, D. Q. Zeng, X. L. Liu, L. S. Wang and D. L. Peng, *Mater. Chem. Phys.*, 2017, **192**, 339–348.

14 J. Guo, H. X. Song, H. Liu, C. J. Luo, Y. R. Ren and T. Ding, *J. Mater. Chem. C*, DOI: 10.1039/c7tc01502j.

15 M. Zhou, X. Zhang, J. M. Wei, S. L. Zhao, L. Wang and B. X. Feng, *J. Phys. Chem. C*, 2010, **115**, 1398–1402.

16 S. He, G. S. Wang, C. Lu, J. Liu, B. Wen, H. Liu, L. Guo and M. S. Cao, *J. Mater. Chem. A*, 2013, **1**, 4685–4692.

17 R. B. Wu, K. Zhou, Z. H. Yang, X. K. Qian, J. Wei, L. Liu, Y. Z. Huang, L. B. Kong and L. Y. Wang, *CrystEngComm*, 2013, **15**, 570–576.

18 F. Xia, J. W. Liu, D. Gu, P. F. Zhao, J. Zhang and R. C. Che, *Nanoscale*, 2011, **3**, 3860–3867.

19 P. T. Xie, K. Sun, Z. Y. Wang, Y. Liu, R. H. Fan, Z. D. Zhang and G. Schumacher, *J. Alloys Compd.*, DOI: 10.1016/j.jallcom.2017.04.248.

20 Y. B. Zhang, P. Wang, Y. Wang, L. Qiao, T. Wang and F. Li, *J. Mater. Chem. C*, 2015, **3**, 10813–10818.

21 W. W. Liu, H. Li, Q. P. Zeng, H. N. Duan, Y. P. Guo, X. F. Liu, C. Y. Sun and H. Z. Liu, *J. Mater. Chem. A*, 2015, **3**, 3739–3747.

22 X. H. Li, J. Feng, Y. P. Du, J. T. Bai, H. M. Fan, H. L. Zhang, Y. Peng and F. S. Li, *J. Mater. Chem. A*, 2015, **3**, 5535–5546.

23 K. Sun, R. H. Fan, Y. S. Yin, J. Guo, X. F. Li, Y. H. Lei, L. Q. An, C. B. Cheng and Z. H. Guo, *J. Phys. Chem. C*, 2017, **121**, 7564–7571.

24 X. J. Zeng, B. Yang, L. Y. Zhu, H. Z. Yang and R. H. Yu, *RSC Adv.*, 2016, **6**, 105644.

25 J. P. Salvetat, A. J. Kulik, J. A. Bonard, J. M. Bonard, G. A. D. Briggs, T. Stockli, K. Metenier, S. Bonnamy and F. Beguin, *Adv. Mater.*, 1999, **11**, 161–165.

26 C. B. Cheng, R. H. Fan, Y. R. Ren, T. Ding, L. Qian, J. Guo, X. F. Li, L. Q. An, Y. H. Lei, Y. S. Yin and Z. H. Guo, *Nanoscale*, DOI: 10.1039/c7nr01516j.

27 Z. D. Zhang, Z. C. Shi, R. H. Fan, M. Gao, J. Y. Guo, X. G. Qi and K. N. Sun, *Mater. Chem. Phys.*, 2011, **130**, 615–618.

28 F. S. Wen, F. Zhang and Z. Y. Liu, *J. Phys. Chem. C*, 2011, **115**, 14025–14030.

29 C. Y. Zhao, A. B. Zhang, Y. P. Zheng and J. F. Luan, *Mater. Res. Bull.*, 2012, **47**, 217–221.

30 Y. Chen, X. Y. Liu, X. Y. Mao, Q. X. Zhang, Z. Xie and Z. W. Han, *Nanoscale*, 2014, **6**, 6440–6447.

31 L. Y. Zhu, X. J. Zeng, B. Yang, X. P. Li and R. H. Yu, *J. Magn. Magn. Mater.*, 2016, **426**, 114–120.

32 X. L. Zheng, J. Feng, Y. Zong, H. Miao, X. Y. Hu, J. T. Bai and X. H. Li, *J. Mater. Chem. C*, 2015, **3**, 4452–4463.

33 X. J. Zeng, B. Yang, X. P. Li, R. F. Li and R. H. Yu, *Mater. Des.*, 2016, **101**, 35–43.

34 G. H. Pan, J. Zhu, S. l. Ma, G. B. Sun and X. J. Yang, *ACS Appl. Mater. Interfaces*, 2013, **5**, 12716–12724.

35 T. T. Chen, F. Deng, J. Zhu, C. F. Chen, G. B. Sun, S. L. Ma and X. J. Yang, *J. Mater. Chem. C*, 2012, **22**, 15190–15197.

36 G. Li, T. S. Xie, S. L. Yang, J. H. Jin and J. M. Jiang, *J. Phys. Chem. C*, 2012, **116**, 9196–9201.

37 H. B. Zhao, Z. B. Fu, H. B. Chen, M. L. Zhong and C. Y. Wang, *ACS Appl. Mater. Interfaces*, 2016, **8**, 1468–1477.

38 K. Sun, R. H. Fan, Z. D. Zhang, K. L. Yan, X. H. Zhang, P. T. Xie, M. X. Yu and S. B. Pan, *Appl. Phys. Lett.*, 2015, **106**, 1729021.

39 Q. Hou, K. Sun, P. T. Xie, K. Yan, R. H. Fan and Y. Liu, *Mater. Lett.*, 2016, **169**, 86–89.

40 N. Li, G. W. Huang, Y. Q. Li, H. M. Xiao, Q. P. Feng, N. Hu and S. Y. Fu, *ACS Appl. Mater. Interfaces*, 2016, **10**, 2973–2983.

41 X. M. Zhang, G. B. Ji, W. Liu, X. X. Zhang, Q. G. Gao, Y. C. Li and Y. W. Du, *J. Mater. Chem. C*, 2016, **4**, 1860–1870.

42 L. N. Wang, X. L. Jia, Y. F. Li, F. Yang, L. Q. Zhang, L. P. Liu, X. Ren and H. T. Yang, *J. Mater. Chem. A*, 2014, **2**, 14940–14946.

43 Y. C. Du, W. W. Liu, R. Qiang, Y. Wang, X. J. Han, J. Ma and P. Xu, *ACS Appl. Mater. Interfaces*, 2014, **6**, 12997–13006.

44 X. L. Dong, X. F. Zhang, H. Huang and F. Zuo, *Appl. Phys. Lett.*, 2008, **92**, 013127.

45 T. Wu, Y. Liu, X. Zeng, T. T. Cui, Y. T. Zhao, Y. N. Li and G. X. Tong, *ACS Appl. Mater. Interfaces*, 2016, **8**, 7370–7380.

46 Y. C. Yin, X. F. Liu, X. J. Wei, R. H. Yu and J. L. Shui, *ACS Appl. Mater. Interfaces*, 2016, **8**, 34686–34698.

47 L. Wang, H. L. Xing, S. T. Gao, X. L. Ji and Z. Y. Shen, *J. Mater. Chem. C*, 2017, **5**, 2005–2014.

48 Z. H. Yang, H. L. Lv and R. B. Wu, *Nano Res.*, 2016, **9**, 3671–3682.

49 H. L. Lv, G. B. Ji, W. Liu, H. Q. Zhang and Y. W. Du, *J. Mater. Chem. C*, 2015, **3**, 10232–10241.

50 D. L. Zhao, X. Li and Z. M. Shen, *J. Alloys Compd.*, 2009, **471**, 457–460.

51 R. B. Yang, P. M. Reddy, C. J. Chang, P. A. Chen and C. C. Chang, *Chem. Eng. J.*, 2016, **285**, 497–507.

52 H. L. Lv, G. B. Ji, H. Q. Zhang and Y. W. Du, *RSC Adv.*, 2015, **5**, 76836–76843.

53 M. S. Cao, J. Yang, W. L. Song, D. Q. Zhang, B. Wen, H. B. Jin, Z. L. Hou and J. Yuan, *ACS Appl. Mater. Interfaces*, 2012, **4**, 6949–6956.